DMD Fast Forward. Published on June 25, 2020 as DOI: 10.1124/dmd.120.000068
This article has not been copyedited and formatted. The final version may differ from this version.

DMD-AR-2020-000068

Title Page

Contribution of monocarboxylate transporter 6 (Mct6) to the pharmacokinetics and pharmacodynamics of bumetanide in mice

Authors: Robert S. Jones [1,3], Donna Ruszaj [1], Mark D. Parker [2], and Marilyn E. Morris [1]

[1] Department of Pharmaceutical Sciences, School of Pharmacy and Pharmaceutical Sciences, University at Buffalo, State University of New York, Buffalo, New York 14214, USA

[2] Department of Physiology and Biophysics, Jacobs School of Medicine and Biomedical Sciences, University at Buffalo, State University of New York, Buffalo, New York 14203, USA

[3] Current address is Drug Metabolism and Pharmacokinetics, Genentech, Inc., South San Francisco, CA, 94080

DMD Fast Forward. Published on June 25, 2020 as DOI: 10.1124/dmd.120.000068
This article has not been copyedited and formatted. The final version may differ from this version.

Running title page

Monocaboxylate transporter 6 and bumetanide pharmacokinetics

Correspondence should be addressed to:

Marilyn E. Morris, PhD

Department of Pharmaceutical Sciences

University at Buffalo

State University of New York

304 Pharmacy Building

Buffalo, NY 14214

Ph: (716) 645-4839

Fax: (716) 829-6569

memorris@buffalo.edu

Number of text pages: 20

Number of tables: 3

Number of figures: 7

Number of references: 33

Abstract: 233 words

Introduction: 631 words

Discussion: 962 words

Nonstandard Abbreviations: AUC: area under the curve, CL: clearance, C_{max}: maximum plasma concentration, cRNA: capped sense RNA, F: bioavailability, f_e: fraction eliminated unchanged in the urine, LC/MS: Liquid chromatography/mass spectrometry, MCT: monocarboxylate transporter, NKCC: sodium-potassium-chloride cotransporter, PD: pharmacodynamics, PK: pharmacokinetics.

DMD Fast Forward. Published on June 25, 2020 as DOI: 10.1124/dmd.120.000068
This article has not been copyedited and formatted. The final version may differ from this version.

Abstract: Bumetanide, a sulfamyl loop diuretic, is used for the treatment of edema in association with congestive heart failure. Being a polar, anionic compound at physiological pH, bumetanide uptake and efflux into different tissues is largely transporter-mediated. Of note, organic anion transporters (OAT; SLC22A) have been extensively studied in terms of their importance in transporting bumetanide to its primary site of action in the kidney. The contribution of one of the less-studied bumetanide transporters, monocarboxylate transporter 6 (MCT6; SLC16A5), to bumetanide pharmacokinetics (PK) and pharmacodynamics (PD) has yet to be characterized. The affinity of bumetanide for murine Mct6 was evaluated using Mct6-transfected *Xenopus laevis* oocytes. Furthermore, bumetanide was intravenously and orally administered to wildtype mice ($Mct6^{+/+}$) and homozygous Mct6 knockout mice ($Mct6^{-/-}$) to elucidate the contribution of Mct6 to bumetanide PK/PD *in vivo*. We demonstrated that murine Mct6 transports bumetanide at a similar affinity compared with human MCT6 (78 and 84 μM, respectively, at pH 7.4). Following bumetanide administration, there were no significant differences in plasma PK. Additionally, diuresis was significantly decreased by ~55% after intravenous bumetanide administration in $Mct6^{-/-}$ mice. Kidney cortex concentrations of bumetanide were decreased, suggesting decreased Mct6-mediated bumetanide transport to its site of action in the kidney. Overall, these results suggest that Mct6 does not play a major role in the plasma PK of bumetanide in mice; however, it significantly contributes to bumetanide's pharmacodynamics due to changes in kidney concentrations.

Significance Statement: Previous evidence suggested that MCT6 transports bumetanide *in vitro*; however, no studies to date have evaluated the *in vivo* contribution of this transporter. *In vitro* studies indicated that mouse and human MCT6 transport bumetanide with similar affinities. Using Mct6 knockout mice, we demonstrated that murine Mct6 does not play a major role in the plasma pharmacokinetics of bumetanide; however, the pharmacodynamic effect of diuresis was attenuated in the knockout mice, likely due to the decreased bumetanide concentrations in the kidney.

DMD Fast Forward. Published on June 25, 2020 as DOI: 10.1124/dmd.120.000068
This article has not been copyedited and formatted. The final version may differ from this version.

Introduction: Bumetanide is a commonly used, potent loop diuretic for the treatment of congestive heart failure. Its primary mechanism of action is through the inhibition of the sodium-potassium-chloride cotransporter (NKCC), more specifically NKCC2 (SLC12A1), which is expressed in the thick ascending limb of the loop of Henle in the kidney (Lytle et al., 1995; Haas and Forbush, 1998). This electroneutral transporter facilitates the absorption of one sodium, one potassium, and two chloride ions across the plasma membrane, which affects ion homeostasis in both blood and urine. Thus, the major pharmacodynamic effects resulting from the inhibition of this transporter are increased diuresis and decreased blood pressure due to decreased tubular sodium reabsorption, which can effectively decrease blood pressure. Bumetanide has also been shown to be a selective inhibitor of NKCC1 (SLC12A2), a more ubiquitously expressed isoform of recent interest due to its neuronal expression and overexpression in diseases such as neonatal seizures and temporal lobe epilepsy (Blaesse et al., 2009; Kahle et al., 2009; Mao et al., 2012; Puskarjov et al., 2014). Consequently, there are several completed and ongoing clinical trials investigating bumetanide as a treatment for various neurological disorders (NCT03899324, NCT00830531, NCT03156153).

Considering the popularity of bumetanide as a treatment for heart failure and repurposing for neurological disorders, the pharmacokinetics of bumetanide have been evaluated using several preclinical rodent models, as well as humans (Holazo et al., 1984; Cook et al., 1988; Han et al., 1993; Weaver et al., 2001; Cleary et al., 2013). Due to the weak acidic nature of the carboxylic acid moiety in bumetanide (pKa = 3.6) (Fig. 1), the compound is negatively ionized at physiological pH which highlights the contribution of drug transporters to its absorption, distribution, and elimination. In humans, basolateral organic anion transporters 1/3 (OAT1/3) and apical OAT4 in the kidney have been widely accepted as the major transporters involved in

DMD Fast Forward. Published on June 25, 2020 as DOI: 10.1124/dmd.120.000068
This article has not been copyedited and formatted. The final version may differ from this version.

the availability of bumetanide to its NKCC2 site of action (Hasannejad et al., 2004). In addition, bumetanide is primarily eliminated via metabolism, and hepatocyte uptake by hepatic sinusoidal OAT2 is likely to play a major role in its transport into the liver for metabolism (Kobayashi et al., 2005). Less is known about the mechanism of absorption of bumetanide in the intestine; however, absorption has been shown to be rapid due to its onset of action in 30 min to 1 hour. Due to the high plasma protein binding of bumetanide (> 95%), it is expected that the unbound systemic concentrations are in the low micromolar range following oral and i.v. administration.

There has been interest in investigating the contribution of organic anion transporters due to their importance in moderating tissue-specific concentrations of bumetanide (Murakami et al., 2005; Romermann et al., 2017). One such transporter, monocarboxylate transporter 6 (MCT6, SLC16A5), has been less studied compared to the other bumetanide transporters. Previous evidence suggested that MCT6 is expressed in major absorption, distribution, metabolism, and excretion (ADME)-related tissues (i.e. kidney, liver, and intestine) and transports a wide variety of substrates similar to that of the OAT solute carrier family, including bumetanide, probenecid, nateglinide, and prostaglandin $F_{2\alpha}$ (Gill et al., 2005; Murakami et al., 2005; Kohyama et al., 2013). While our lab and others have demonstrated that bumetanide is a substrate of human MCT6 (Murakami et al., 2005; Jones et al., 2017), no study has yet investigated the significance Mct6 plays in bumetanide transport and its pharmacokinetics/pharmacodynamics (PK/PD). Therefore, the purpose of this study was to investigate the overall contribution of Mct6 in the PK and PD of bumetanide in mice. Firstly, the *in vitro* transporter kinetic parameters (K_t and J_{max}) were characterized using murine Mct6-transfected *Xenopus laevis* oocytes. Secondly, bumetanide was administered following oral and i.v. administrations to wildtype ($Mct6^{+/+}$) and

DMD Fast Forward. Published on June 25, 2020 as DOI: 10.1124/dmd.120.000068
This article has not been copyedited and formatted. The final version may differ from this version.

Mct6-knockout ($Mct6^{-/-}$) mice to compare PK parameters (clearance, bioavailability) and a measure of bumetanide pharmacodynamics (24-hour diuresis).

DMD Fast Forward. Published on June 25, 2020 as DOI: 10.1124/dmd.120.000068
This article has not been copyedited and formatted. The final version may differ from this version.

Materials and Methods:

Chemicals. Bumetanide (≥ 98% purity) was purchased from Sigma-Aldrich (St. Louis, MO). All other chemicals and HPLC-grade reagents were purchased from Fisher Scientific (Hampton, NH). Deuterated bumetanide (bumetanide-d5) used as the internal standard was purchased from Santa Cruz Biotechnology (Santa Cruz CA).

Animals. C56BL/6NCr Mct6$^{+/+}$ wildtype mice (Charles River, Wilmington, MA) and previously generated Mct6$^{-/-}$ knockout mice were used throughout this study (Jones et al., 2019). Body weights throughout the studies ranged from 17-35 g and ages ranged from 8-19 weeks old. All mice were housed in cages with a 12 h light/12 h dark cycle. Animals were given free access to normal chow (Envigo 2018 Teklad global 18% protein extruded rodent diet) *ad libitum* and water. Experiments were conducted following approval of the Institution of Animal Use and Care Committee, University at Buffalo. Male mice were used in all studies.

Transfection of murine Mct6 in X. laevis oocytes. Murine Mct6 was transfected into prepared *X. laevis* oocytes as described previously (Jones et al., 2017; Jones et al., 2020). Briefly, murine Mct6 cRNA was transcribed from *NotI*-linearized pGH19-Mct6 vector using the mMESSAGE mMACHINE T7 transcription kit. Approximately 13.8 nL of cRNA or water was injected into oocytes isolated from digested, resected ovaries the day before. The oocytes were then incubated in OR3 medium at 18°C for 3 to 5 days for *in vitro* experiments. OR3 medium was prepared as described previously (Musa-Aziz et al., 2010). All cRNA was verified for purity, concentration, stability, and correct size prior to injection.

DMD Fast Forward. Published on June 25, 2020 as DOI: 10.1124/dmd.120.000068
This article has not been copyedited and formatted. The final version may differ from this version.

Bumetanide uptake studies. The uptake studies were performed, as previously described. . Time and concentration-dependent uptake studies were performed using groups of 4 to 5 oocytes in 24-well multi-dishes which were preincubated in uptake buffer (15 mM HEPES, 82.5 mM NaCl, 2.5 mM KCl, 1 mM Na_2HPO_4, and 1 mM $MgCl_2$, adjusted to pH 7.4 with Tris) for 30 min. For the time-dependent study, the oocytes were transferred to 400 µL of uptake buffer containing 0.1 µM bumetanide, and the oocytes were incubated at pH 7.4 at room temperature (~20-23°C). For the concentration-dependent study, bumetanide concentrations were varied and the uptake time was chosen to be in the linear range of the time-dependent study (60 min). All uptake was stopped by the addition of ice-cold uptake buffer, and the oocytes were washed three times. Individual oocytes were placed in separate scintillation vials and dissolved in 250 µl of 10% sodium lauryl sulfate by slowly shaking for 1.5 h. Radioactivity was determined by liquid scintillation counting following the addition of scintillation cocktail.

Pharmacokinetic and pharmacodynamics studies with bumetanide in mice. C57BL/6NCr $Mct6^{+/+}$ and $Mct6^{-/-}$ mice were fasted overnight prior to the experiments and throughout the study. The i.v. and oral (p.o.) doses of bumetanide were chosen to be within a safe and efficacious range to reliably measure the pharmacokinetics (PK) and pharmacodynamics (PD) of the drug. Based on previous experiments in mice and rats (Lee et al., 1994; Kim and Lee, 2001; Brandt et al., 2010; Topfer et al., 2014), 1 and 10 mg/kg i.v. and 2.5 and 25 mg/kg p.o. were chosen as the doses for this study. No adverse events or toxicity for these doses was reported in the literature and the LD_{50} for oral bumetanide administration in mice was reported to be much higher (4.6 g/kg). Similarly to previous studies (Lee et al., 1994; Brandt et al., 2010; Topfer et al., 2014), bumetanide was dissolved in a small volume of 0.1 N NaOH and diluted with 0.9%

saline, and filtered through a 0.45 µm filter; volumes of 3 mL/kg were used for i.v. injection and 8 mL/kg for p.o. administration. Previous studies showed that this dosing formulation did not produce differences in bumetanide PK/PD from other dosing formulations (Lee et al., 1994; Topfer et al., 2014). Doses were administered as retro-orbital injections for i.v. and via oral gavage for p.o. doses. Blood was sampled at 5, 15, 30, 45, 60, 120, 240, and 300 min post-dose via sub-mandibular puncture. Plasma was collected following centrifugation and stored at -80ºC until analysis. Urine was collected over a 24-hour period using metabolic cages (Tecniplast, Buguggiate, Italy) and following centrifugation to sediment insoluble material, the volume was measured and the urine samples stored at -80ºC until analysis. Tissues were collected immediately following cardiac puncture, frozen in liquid nitrogen, and stored at -80ºC until analysis.

Plasma and urine sample preparation. Briefly, plasma samples were thawed on ice and 5 µL of internal standard (IS: 20 µg/mL bumetanide-d5) was added to 20 µL of sample. Protein was precipitated by the addition of 400 µL of 0.1% formic acid in acetonitrile. The mixture was vortexed, sonicated, and centrifuged at 12,750 x g at 4ºC for 10 min to sediment the precipitate. The supernatant (370 µL) was added to 630 µL of water in an LC/MS vial, vortexed, and used for analysis. For urine, 5 µL of IS was added to 50 µL of sample thawed on ice. Protein was precipitated by the addition of 300 µL of 0.1% formic acid in acetonitrile. The mixture was vortexed, sonicated, and centrifuged at 12,750 x g at 4ºC for 10 min to sediment the precipitate. The supernatant (300 µL) was added to 300 µL of water in an LC/MS vial, vortexed, and used for analysis. For urine, $A_{e,24\text{-}hr}$ was calculated by multiplying the concentration of bumetanide by the volume of each urine sample.

DMD Fast Forward. Published on June 25, 2020 as DOI: 10.1124/dmd.120.000068
This article has not been copyedited and formatted. The final version may differ from this version.

Liver and kidney sample preparation. Briefly, whole liver tissue was homogenized in 5/95 *v/v* methanol/water (5 mL/g). Subsequently, 5 µL of IS was added to 100 µL of homogenate. Protein was precipitated by the addition of 800 µL of 1% formic acid in acetonitrile. The mixture was vortexed, sonicated, and centrifuged at 12,750 RPM at 4°C for 10 min. For the solid phase extraction, Oasis HLB Prime cartridges were conditioned with 0.5 mL of 1% formic acid in acetonitrile and 0.5 mL of 90/10 acetonitrile/water. For elution, 840 µL of sample supernatant was loaded onto the column and the eluent was collected in a clean glass tube. The column was further rinsed two times with 0.5 mL of 90/10 acetonitrile/water and the eluent was additionally collected. This total eluent was evaporated to dryness under nitrogen, and the sample was reconstituted with 300 µL of 50/50 acetonitrile/water with vortexing. The final solution was centrifuged at 12,750 RPM at 4°C for 5 min to remove insoluble material. The supernatant was transferred to an LC/MS vial for analysis.

Similarly, for kidney cortex samples, the outer layer of a kidney (~40 mg) was collected by sectioning with a razor, and prepared in the same manner as liver samples. However, following protein precipitation and sedimentation, 800 µL of sample supernatant was transferred to a clean glass tube and evaporated to dryness under nitrogen. The sample was reconstituted with 300 µL of 50/50 acetonitrile/water with vortexing, followed by removal of insoluble material and transfer of the supernatant to an LC/MS vial for analysis.

LC/MS/MS and chromatographic conditions. The LC/MS/MS assay was performed on Shimadzu Prominence HPLC with binary pump and autosampler (Shimadzu Scientific, Marlborough, MA) connected to a Sciex API 3000 triple quadruple tandem mass spectrometer

DMD Fast Forward. Published on June 25, 2020 as DOI: 10.1124/dmd.120.000068
This article has not been copyedited and formatted. The final version may differ from this version.

with electrospray ionization (ESI) (Sciex, Foster City, CA). Chromatographic separation was achieved by injecting 10 µL of the sample onto a SymmetryShield RP8 2.1 mm X 100 mm, 3.5 µm particle size (Waters, Milford, MA). Mobile phase A consisted of acetonitrile/water (5/95, *v/v*) with 0.1% formic acid and mobile phase B was acetonitrile/water (95/5, *v/v*) with 0.1% formic acid. The flow rate was 200 µl/min with a gradient elution profile and a total run time of 13 min. The gradient starts at 50% B and increases to 95% over 5 minutes. It was then held at 95% B for 3minutes before returning to the starting conditions of 50% B. The mass spectrometer was operated in multiple reaction monitoring (MRM) mode utilizing ESI for specific detection of bumetanide and d-5 bumetanide as the internal standard. The mrm transitions monitored were 365.3/240.1 for bumetanide and 370.3./245.2 for the d-5 bumetanide. The mass spectrometer parameters were optimized for maximum sensitivity: declustering potential 38 V, entrance potential 10 V, collision energy 22 V and collision cell exit potential of 20 V. The ion spray voltage was +5500 V and the source temperature was 350◦C. The data was analyzed using Analyst version 1.4.2 (Sciex, Foster City, CA).

Assay validation and lower limits of quantification. The calibration curves for analyzing bumetanide concentrations were linear from 0.0125 - 175 µg/mL, 0.005 - 70.0 µg/mL, 5 - 12500 ng/g, and 10 - 25000 ng/g for plasma, urine, liver, and kidney tissue respectively ($R^2 \geq 0.999$). For plasma, the LLOQ values for bumetanide in these matrices were 0.0125 µg/mL, 0.005 µg/mL, 5 ng/g, and 10 ng/g for plasma, urine, liver, and kidney tissue respectively. LC/MS validations are presented in Supplemental Tables 1-4.

DMD Fast Forward. Published on June 25, 2020 as DOI: 10.1124/dmd.120.000068
This article has not been copyedited and formatted. The final version may differ from this version.

Data analysis and statistics. Time-dependent bumetanide uptake rate (µl/oocyte) was calculated as the ratio of radioactivity in each sample (dpm/oocyte) to the initial concentration in the uptake buffer (dpm/µl). All murine Mct6-mediated uptake was calculated as the difference between the murine Mct6 cRNA-injected oocytes and the water-injected oocytes. Data analysis was performed using GraphPad Prism 7 (GraphPad Software Inc., San Diego CA). The concentration-dependent bumetanide uptake rate (pmol/oocyte/hr) was calculated as the ratio of radioactivity in each sample (dpm/oocyte) to the concentration in the uptake buffer (dpm/pmol). The kinetic parameters of concentration-dependent uptake of bumetanide was calculated by fitting with the equation below (Eq. 1) using weighted nonlinear regression analysis (ADAPT 5; Biomedical Simulations Research, University of South California, Los Angeles, CA).

$$J = \frac{J_{max} \cdot C}{K_t + C} \quad (1)$$

Where J is the Mct6-mediated uptake rate, C is the concentration of substrate (µM), J_{max} is the maximum uptake rate, and K_t is the substrate concentration at the half-maximal uptake rate (µM).

For bumetanide pharmacokinetic parameters, non-compartmental analysis (NCA) was performed in Phoenix WinNonlin 7.0 (Pharsight, Mountain View, CA). Oral bioavailability (F) was calculated using Eq. 2

$$F = \frac{D_{iv} \cdot AUC_{po}}{D_{po} \cdot AUC_{iv}} \quad (2)$$

where D is dose and AUC is area under the curve from time zero to infinite ($AUC_{0-\infty}$)

For i.v. doses, the fraction eliminated unchanged in the urine (f_e) was calculated by dividing $A_{e,24\text{-hr}}$ by the dose for each mouse individually and then reported as mean ± S.D. For oral doses, f_e was calculated by dividing $A_{e,24\text{-hr}}$ by the dose multiplied by F for each mouse individually and then reported as mean ± S.D. The observed maximum plasma concentration

(C_{max}) was also determined following oral administration. Renal clearance (CL_R) was calculated by multiplying total plasma clearance (CL) by f_e. Non-renal clearance (CL_{NR}) was calculated by subtracting CL_R from CL. All statistical analyses were performed using an unpaired Student t-test or the one-way unpaired analysis of variance (ANOVA) followed by Dunnett's test to test for multiple comparisons.

DMD Fast Forward. Published on June 25, 2020 as DOI: 10.1124/dmd.120.000068
This article has not been copyedited and formatted. The final version may differ from this version.

Results:

Mct6 transported bumetanide at similar affinity as human MCT6. The results from the time and concentration-dependent uptake of bumetanide for murine Mct6 are presented in Fig. 2. Uptake of 0.1 μM bumetanide at pH 7.4 and RT was in the linear range of uptake (Fig. 2A) prior to steady state at approximately 180 min. Therefore, for the purpose of the concentration-dependent uptake studies, 60 min was used as the uptake time. By fitting with Eq. (1), the transporter kinetic parameters (K_t, J_{max}) for murine Mct6-mediated (Fig. 2B) transport of bumetanide were calculated. At pH 7.4, the affinity (K_t) was 77.6 ± 12.6 μM and the maximal capacity (J_{max}) was 258 ± 35.3 pmol/oocyte/hr.

Plasma pharmacokinetics of bumetanide in wildtype Mct6$^{+/+}$ mice. Following i.v. (1 and 10 mg/kg) and p.o. (2.5 and 25 mg/kg) administration, bumetanide exhibited apparent biphasic PK (Fig. 3), and no major changes were observed in dose-normalized $AUC_{0-\infty}$ estimates from the non-compartmental analysis (NCA) (Table 1). In addition, there were no changes in CL or F at these doses, suggesting that the absorption and elimination of bumetanide at different routes of administration were also linear in mice. The average termination half-life for bumetanide after intravenous administration in mice was calculated to be ~35 min, which is similar to what was reported in the literature (47 min) (Topfer et al., 2014). Following oral administration, while absorption appeared to be rapid (C_{max} ≤ 15 min), the terminal half-life was much longer compared to that after i.v. administration.

Comparative plasma pharmacokinetics of bumetanide in Mct6$^{+/+}$ and Mct6$^{-/-}$ mice. To investigate the contribution of Mct6 on the plasma PK of bumetanide, bumetanide was

DMD Fast Forward. Published on June 25, 2020 as DOI: 10.1124/dmd.120.000068
This article has not been copyedited and formatted. The final version may differ from this version.

administered at 10 mg/kg i.v. and 25 mg/kg p.o. to the $Mct6^{-/-}$ and $Mct6^{+/+}$ mice. (Fig. 4). For i.v. administration, there were no statistically significant differences between the AUC, CL, or terminal half-life (Table 1). After oral administration, the $AUC_{0\text{-}300min}$ and C_{max} both decreased (by 15% and 37%, respectively), although there were no statistically significant differences likely due to the observed large variability (Table 2).

Urinary elimination of bumetanide and diuresis in $Mct6^{+/+}$ and $Mct6^{-/-}$ mice. As depicted in Fig. 5, there were no significant differences in the $A_{e,24\text{-}hr}$ between the two groups of mice for the highest i.v. and p.o. doses in the $Mct6^{+/+}$ and $Mct6^{-/-}$ mice (Table 3). CL_R accounted for < 25% in all cases suggesting that the urinary elimination of bumetanide plays a minor role in the total clearance of bumetanide in mice. Upon measuring the volume of urine excreted 24 hours post dose administration (diuresis) (Fig. 6), there was a significant difference between the $Mct6^{-/-}$ and wildtype $Mct6^{+/+}$ mice following i.v. administration (~55% decrease in $Mct6^{-/-}$ mice).

Impact of Mct6 on liver and kidney concentrations of bumetanide. To investigate the impact of Mct6 on the exposure of bumetanide to major tissues involved in bumetanide's PK/PD, liver and kidney concentrations of bumetanide were evaluated following oral and i.v. administration respectively. Fig. 7A shows a decrease in liver bumetanide concentrations 60 min following a 25 mg/kg p.o. dose in the $Mct6^{-/-}$ compared with $Mct6^{+/+}$ mice; however, this decrease was not significant (p = 0.431). In addition, kidney cortex concentrations of bumetanide, determined 30 min following a 10 mg/kg i.v. dose, exhibited a statistically significant 35% decrease in the $Mct6^{-/-}$ mice compared to $Mct6^{+/+}$ mice (Fig. 7B).

DMD Fast Forward. Published on June 25, 2020 as DOI: 10.1124/dmd.120.000068
This article has not been copyedited and formatted. The final version may differ from this version.

Discussion: In this study, we investigated the contribution of Mct6 to the PK/PD of bumetanide in mice. Previously, Murakami et al. suggested that Mct6 may play a role in the transport of bumetanide *in vivo* due to the predicted lack of saturation of human MCT6 at physiological concentrations of bumetanide (Murakami et al., 2005). In order to confirm this in mice, the affinity for murine Mct6 for bumetanide was determined to be 78 µM, which was very similar to what was reported for human MCT6 at physiological pH (84 µM) (Murakami et al., 2005). Prior to investigating potential changes of bumetanide PK in $Mct6^{-/-}$ mice, bumetanide PK was evaluated in wildtype $Mct6^{+/+}$ mice using two different oral and intravenous doses. The PK appeared to be biphasic and linear, with no apparent changes in total plasma clearance or bioavailability with changes in dose. The terminal half-life of bumetanide after i.v. administration in mice was similar to what was reported in previous studies in mice (Topfer et al., 2014; Tollner et al., 2015) (~30-50 min). The half-life is somewhat shorter than what is reported for humans (~ 1 hr) (Dixon et al., 1976). Similar kinetics have been reported in other species including rat (Lee et al., 1994), dog (Smith and Lau, 1983), and monkey and baboons (Walmsley, 1985), which all demonstrated polyexponential elimination. Additionally, the long terminal half-life following oral administration seen in our data was also demonstrated in baboons, which suggests absorption-limited elimination following oral doses of bumetanide. This phenomenon was also reported in humans (Brater et al., 1984).

Studies of bumetanide PK in $Mct6^{-/-}$ mice indicated that Mct6 does not significantly influence the plasma PK in mice following oral and intravenous administration. While decreases in C_{max}, AUC, and liver concentrations of bumetanide were observed following oral administration in $Mct6^{-/-}$ mice, these changes were not significant. These data suggest that Mct6 may play only a minor role in the first-pass absorption of bumetanide in mice at the doses used in

DMD Fast Forward. Published on June 25, 2020 as DOI: 10.1124/dmd.120.000068
This article has not been copyedited and formatted. The final version may differ from this version.

this study. However, further studies are needed prior to drawing these conclusions, partly due to the large variability in the oral PK data. In addition, considering that our $AUC_{0\text{-}300min}$ and $AUC_{0\text{-}\infty}$ were greater than 40% different after oral administration, further terminal data is required to confirm the terminal plasma concentrations of bumetanide following oral administration.

The diuretic effect of bumetanide was significantly attenuated following intravenous bumetanide administration in $Mct6^{-/-}$ mice compared to wildtype mice; decreased urinary excretion was also observed after oral administration in $Mct6^{-/-}$ mice, but changes were not significant, likely due to the larger variability compared with i.v. administration. Assuming the fraction unbound of bumetanide in mice is similar to what is estimated in rats (f_{up} ~ 0.02) (Kim and Lee, 2001), the clearance mediated by renal filtration (CL_{RF}) can be estimated via glomerular filtration rate (GFR) (which is estimated to be ~260 µL/min (Levine et al., 2006)) multiplied by f_{up}. Considering the average weight of a mouse in this study is ~26 g, the CL_{RF} is ~0.21 mL/min/kg for bumetanide. Therefore, active renal secretion (CL_{RS}) of bumetanide is a major component of its total renal clearance (which is estimated to be greater than 0.6 mL/min/kg). While renal clearance of bumetanide is not a major route of elimination in mice, it is important to note that its distribution and diuretic effect in the kidney may still be impacted by changes in renal disposition. It is possible that Mct6 plays a role in the secretion of bumetanide into the cortical renal cells, a site of action of bumetanide's inhibition of NKCC2, to exhibit its diuretic effect. This is supported by the fact that bumetanide concentrations in kidney cortex were significantly decreased in $Mct6^{-/-}$ mice following a 10 mg/kg i.v. dose at 30 min post-administration. However, further kidney concentration data, as well as the evaluation of changes in other determinants of kidney tissue concentrations, are necessary to confirm this hypothesis. Mct6 mRNA is expressed in kidney, but its protein expression and localization in the kidney

(basolateral versus brush-border membrane localization) is unknown. Further studies are necessary to elucidate the function of Mct6 in the kidney.

It is also important to note that systemic concentrations of bumetanide in humans range from ng/mL to µg/mL(Pentikainen et al., 1977; Holazo et al., 1984), similar to the range of concentrations observed in the present studies. In addition, the bioavailability and overall elimination of bumetanide is different between rodents and humans. In humans, it is reported that the bioavailability of bumetanide is approximately 80% (Holazo et al., 1984), while in mice we found it to be much less (~30%). This is most likely due to the rapid first-pass metabolism of bumetanide in rodents compared to humans via oxidation of the *N*-butyl sidechain (Topfer et al., 2014). In addition, the fraction eliminated unchanged in the urine in mice was calculated to be less than 25% in all cases, compared to humans which showed 60% eliminated as intact parent drug in the urine following a 1 mg oral dose of bumetanide. Due the greater importance of renal clearance of bumetanide in humans, it is possible that human MCT6 may play a more important role in the kidney disposition and pharmacodynamics of bumetanide in humans.

In summary, this study represents the first evidence that Mct6 may play a role in moderating kidney concentrations of bumetanide *in vivo*, which has a downstream impact on the diuresis mediated by bumetanide. This is supported by PK/PD studies performed in our knockout animal model, as well as recent studies performed by Xu et al. that provide evidence for significant bumetanide interactions with rat Mct6 (Xu et al., 2019). Moving forward, additional studies performed with the $Mct6^{-/-}$ model could provide evidence for significant MCT6-mediated drug-drug interactions with other loop diuretics that could impact drug ADME and efficacy.

Acknowledgments.

The authors would like to acknowledge Drs Mark D. Parker, Mark A. Bryniarski, Michael Deci, and Scott Ferguson for their assistance in animal handling.

Authorship Contributions

Participated in research design: Jones, Ruszaj, Parker, and Morris

Conducted experiments: Jones and Ruszaj

Performed data analysis: Jones, Ruszaj and Morris

Wrote or contributed to the writing of the manuscript: Jones, Ruszaj, and Morris

References:

Blaesse P, Airaksinen MS, Rivera C, and Kaila K (2009) Cation-chloride cotransporters and neuronal function. *Neuron* **61:**820-838.

Brandt C, Nozadze M, Heuchert N, Rattka M, and Loscher W (2010) Disease-Modifying Effects of Phenobarbital and the NKCC1 Inhibitor Bumetanide in the Pilocarpine Model of Temporal Lobe Epilepsy. *Journal of Neuroscience* **30:**8602-8612.

Brater DC, Day B, Burdette A, and Anderson S (1984) Bumetanide and furosemide in heart failure. *Kidney international* **26:**183-189.

Cleary RT, Sun H, Huynh T, Manning SM, Li Y, Rotenberg A, Talos DM, Kahle KT, Jackson M, Rakhade SN, Berry G, and Jensen FE (2013) Bumetanide enhances phenobarbital efficacy in a rat model of hypoxic neonatal seizures. *PloS one* **8:**e57148.

Cook JA, Smith DE, Cornish LA, Tankanow RM, Nicklas JM, and Hyneck ML (1988) Kinetics, dynamics, and bioavailability of bumetanide in healthy subjects and patients with congestive heart failure. *Clinical pharmacology and therapeutics* **44:**487-500.

Dixon WR, Young RL, Holazo A, Jack ML, Weinfeld RE, Alexander K, Liebman A, and Kaplan SA (1976) Bumetanide: radioimmunoassay and pharmacokinetic profile in humans. *Journal of pharmaceutical sciences* **65:**701-704.

Gill RK, Saksena S, Alrefai WA, Sarwar Z, Goldstein JL, Carroll RE, Ramaswamy K, and Dudeja PK (2005) Expression and membrane localization of MCT isoforms along the length of the human intestine. *American journal of physiology Cell physiology* **289:**C846-852.

Haas M and Forbush B, 3rd (1998) The Na-K-Cl cotransporters. *Journal of bioenergetics and biomembranes* **30:**161-172.

Han KS, Lee SH, Lee MG, and Kim ND (1993) Pharmacokinetics and pharmacodynamics of bumetanide after intravenous and oral administration to spontaneously hypertensive rats and DOCA-salt induced hypertensive rats. *Biopharmaceutics & drug disposition* **14:**533-548.

Hasannejad H, Takeda M, Taki K, Shin HJ, Babu E, Jutabha P, Khamdang S, Aleboyeh M, Onozato ML, Tojo A, Enomoto A, Anzai N, Narikawa S, Huang XL, Niwa T, and Endou H (2004) Interactions of human organic anion transporters with diuretics. *The Journal of pharmacology and experimental therapeutics* **308:**1021-1029.

Holazo AA, Colburn WA, Gustafson JH, Young RL, and Parsonnet M (1984) Pharmacokinetics of Bumetanide Following Intravenous, Intramuscular, and Oral Administrations to Normal Subjects. *Journal of pharmaceutical sciences* **73:**1108-1113.

Jones RS, Parker MD, and Morris AME (2020) Monocarboxylate Transporter 6-Mediated Interactions with Prostaglandin F2alpha: In Vitro and In Vivo Evidence Utilizing a Knockout Mouse Model. *Pharmaceutics* **12**.

Jones RS, Parker MD, and Morris ME (2017) Quercetin, Morin, Luteolin, and Phloretin Are Dietary Flavonoid Inhibitors of Monocarboxylate Transporter 6. *Molecular pharmaceutics*.

Jones RS, Tu C, Zhang M, Qu J, and Morris ME (2019) Characterization and Proteomic-Transcriptomic Investigation of Monocarboxylate Transporter 6 Knockout Mice: Evidence of a Potential Role in Glucose and Lipid Metabolism. *Molecular pharmacology* **96:**364-376.

Kahle KT, Barnett SM, Sassower KC, and Staley KJ (2009) Decreased seizure activity in a human neonate treated with bumetanide, an inhibitor of the Na(+)-K(+)-2Cl(-) cotransporter NKCC1. *Journal of child neurology* **24:**572-576.

Kim EJ and Lee MG (2001) Pharmacokinetics and pharmacodynamics of intravenous bumetanide in mutant Nagase analbuminemic rats: importance of globulin binding for the pharmacodynamic effects. *Biopharmaceutics & drug disposition* **22:**147-156.

Kobayashi Y, Ohshiro N, Sakai R, Ohbayashi M, Kohyama N, and Yamamoto T (2005) Transport mechanism and substrate specificity of human organic anion transporter 2 (hOat2 [SLC22A7]). *The Journal of pharmacy and pharmacology* **57:**573-578.

Kohyama N, Shiokawa H, Ohbayashi M, Kobayashi Y, and Yamamoto T (2013) Characterization of Monocarboxylate Transporter 6: Expression in Human Intestine and Transport of the Antidiabetic Drug Nateglinide. *Drug Metab Dispos* **41:**1883-1887.

Lee SH, Lee MG, and Kim ND (1994) Pharmacokinetics and pharmacodynamics of bumetanide after intravenous and oral administration to rats: absorption from various GI segments. *Journal of pharmacokinetics and biopharmaceutics* **22:**1-17.

Levine DZ, Iacovitti M, Robertson SJ, and Mokhtar GA (2006) Modulation of single-nephron GFR in the db/db mouse model of type 2 diabetes mellitus. *American journal of physiology Regulatory, integrative and comparative physiology* **290:**R975-981.

Lytle C, Xu JC, Biemesderfer D, and Forbush B, 3rd (1995) Distribution and diversity of Na-K-Cl cotransport proteins: a study with monoclonal antibodies. *The American journal of physiology* **269:**C1496-1505.

Mao S, Garzon-Muvdi T, Di Fulvio M, Chen Y, Delpire E, Alvarez FJ, and Alvarez-Leefmans FJ (2012) Molecular and functional expression of cation-chloride cotransporters in dorsal root ganglion neurons during postnatal maturation. *Journal of neurophysiology* **108:**834-852.

Murakami Y, Kohyama N, Kobayashi Y, Ohbayashi M, Ohtani H, Sawada Y, and Yamamoto T (2005) Functional characterization of human monocarboxylate transporter 6 (SLC16A5). *Drug Metab Dispos* **33:**1845-1851.

Musa-Aziz R, Boron WF, and Parker MD (2010) Using fluorometry and ion-sensitive microelectrodes to study the functional expression of heterologously-expressed ion channels and transporters in Xenopus oocytes. *Methods* **51:**134-145.

Pentikainen PJ, Penttila A, Neuvonen PJ, and Gothoni G (1977) Fate of [14C]-bumetanide in man. *British journal of clinical pharmacology* **4:**39-44.

Puskarjov M, Kahle KT, Ruusuvuori E, and Kaila K (2014) Pharmacotherapeutic targeting of cation-chloride cotransporters in neonatal seizures. *Epilepsia* **55:**806-818.

Romermann K, Fedrowitz M, Hampel P, Kaczmarek E, Tollner K, Erker T, Sweet DH, and Loscher W (2017) Multiple blood-brain barrier transport mechanisms limit bumetanide accumulation, and therapeutic potential, in the mammalian brain. *Neuropharmacology* **117:**182-194.

Smith DE and Lau HS (1983) Determinants of bumetanide response in the dog: effect of probenecid. *Journal of pharmacokinetics and biopharmaceutics* **11:**31-46.

Tollner K, Brandt C, Romermann K, and Loscher W (2015) The organic anion transport inhibitor probenecid increases brain concentrations of the NKCC1 inhibitor bumetanide. *European journal of pharmacology* **746:**167-173.

Topfer M, Tollner K, Brandt C, Twele F, Broer S, and Loscher W (2014) Consequences of inhibition of bumetanide metabolism in rodents on brain penetration and effects of

bumetanide in chronic models of epilepsy. *The European journal of neuroscience* **39:**673-687.

Walmsley L (1985) Pharmacokinetics of bumetanide, lorazepam and clofibric acid in cynomolgus monkeys and baboons, Loughborough University of Technology.

Weaver ML, Orwig BA, Rodriguez LC, Graham ED, Chin JA, Shapiro MJ, McLeod JF, and Mangold JB (2001) Pharmacokinetics and metabolism of nateglinide in humans. *Drug metabolism and disposition: the biological fate of chemicals* **29:**415-421.

Xu F, Zhu L, Qian C, Zhou J, Geng D, Li P, Xuan W, Wu F, Zhao K, Kong W, Qin Y, Liang L, Liu L, and Liu X (2019) Impairment of Intestinal Monocarboxylate Transporter 6 Function and Expression in Diabetic Rats Induced by Combination of High-Fat Diet and Low Dose of Streptozocin: Involvement of Butyrate-Peroxisome Proliferator-Activated Receptor-gamma Activation. *Drug metabolism and disposition: the biological fate of chemicals* **47:**556-566.

Footnotes

This work was supported by the National Institutes of Health National Institute on Drug Abuse [Grant R01DA023223]. RSJ was supported in part by a PhRMA Pre-Doctoral Graduate Fellowship.

DMD Fast Forward. Published on June 25, 2020 as DOI: 10.1124/dmd.120.000068
This article has not been copyedited and formatted. The final version may differ from this version.

Legends for Figures

Fig. 1. Chemical structure of bumetanide.

Fig. 2. Time (A) and concentration-dependent (B) uptake of bumetanide in murine Mct6-transfected *X. laevis* oocytes. (N = 4 – 5 oocytes/data point). Experiment was performed at least three separate times with at least 2 different ovaries. Data are presented as mean ± S.D. Closed circles: murine Mct6 cRNA-injected, open circles: water-injected, open squares: Mct6-mediated uptake (Mct6 cRNA-injected minus water-injected). Dashed line represents model fitting using Eq. (1) to Mct6-mediated uptake data.

Fig. 3. Concentration-time profiles of bumetanide in after i.v. (A) and p.o. (B) administration in $Mct6^{+/+}$ wildtype mice. N = 3-4 mice/group. Data is plotted as mean ± S.D.

Fig. 4. Concentration-time profiles of bumetanide in after 10 mg/kg i.v. (A) and 25 mg/kg p.o. (B) administration in $Mct6^{+/+}$ (closed symbols) and $Mct6^{-/-}$ (open symbols) mice. N = 3-4 mice/group. Data is plotted as mean ± S.D.

Fig. 5. Amount of bumetanide eliminated unchanged in the urine ($A_{e,24\text{-}hr}$) following different dose administrations (i.v.: A and B, p.o.: C and D). Urine was collected following a 24 hour urine collection. N = 4 mice/group. Data is plotted as mean ± S.D. An unpaired Student t-test was performed to test for statistical significance.

Fig. 6. Urinary output following administration of bumetanide. N = 4 mice/group. Data is plotted as mean ± S.D. An unpaired Student t-test was performed to test for statistical significance.

Fig. 7. Bumetanide tissue concentrations in (A) liver at 60 min following a 25 m/kg p.o. dose administration and (B) kidney cortex at 30 min following a 10 m/kg i.v. dose administration. N =

4 mice/group. Data is plotted as mean ± S.D. An unpaired Student t-test was performed to test for statistical significance.

DMD Fast Forward. Published on June 25, 2020 as DOI: 10.1124/dmd.120.000068
This article has not been copyedited and formatted. The final version may differ from this version.

Tables

Route	**IV**		**PO**	
Dose (mg/kg)	**10**	**1**	**25**	**2.5**
$AUC_{0\text{-}300min}$ (µg·min/mL)	1.57×10^3 (142)	159 (11.8)	719 (52.2)	82.0 (9.37)
$AUC_{0\text{-}\infty}$ (µg·min/mL)	1.57×10^3	159	1.16×10^3	122
CL or CL/F[1] (mL/min/kg)	6.37	6.28	21.0	20.6
Terminal $t_{1/2}$ (min)	36.2	34.0	284	224
		F	0.295	0.309

Table 1: Non-compartmental analysis (NCA) of bumetanide PK in $Mct6^{+/+}$ mice (AUC: area under the curve, CL: total plasma clearance, $t_{1/2}$: half-life, F: oral bioavailability). Data are reported as mean values. For $AUC_{0\text{-}300min}$, the S.E.M. values are reported in parentheses. [1]CL/F was reported for oral routes of administration.

DMD Fast Forward. Published on June 25, 2020 as DOI: 10.1124/dmd.120.000068
This article has not been copyedited and formatted. The final version may differ from this version.

Route	IV (10 mg/kg)		PO (25 mg/kg)	
	Mct6$^{+/+}$	**Mct6$^{-/-}$**	**Mct6$^{+/+}$**	**Mct6$^{-/-}$**
$AUC_{0\text{-}300min}$ (µg·min/mL)	1.57 x 10^3 (142)	1.45 x 10^3 (45.3)	719 (52.2)	613 (43.7)
$AUC_{0\text{-}\infty}$ (µg·min/mL)	1.57 x 10^3	1.46 x 10^3	1.16 x 10^3	1.08 x 10^3
CL or CL/F[1] (mL/min/kg)	6.35	6.84	21.0	22.0
Terminal $t_{1/2}$ (min)	36.2	42.6	284	245
		F	0.295	0.295
		C_{max} (µg/mL)	7.45 (1.15)	4.66 (0.917)

Table 2: NCA of bumetanide PK in Mct6$^{+/+}$ and Mct6$^{-/-}$ mice following 10 mg/kg i.v. (IV) and 25 mg/kg p.o. (PO) dose administrations. Data are reported as mean values. For $AUC_{0\text{-}300min}$, the S.E.M. values are reported in parentheses. [1]CL/F was reported for oral routes of administration.

DMD Fast Forward. Published on June 25, 2020 as DOI: 10.1124/dmd.120.000068
This article has not been copyedited and formatted. The final version may differ from this version.

Route	IV (10 mg/kg)		PO (25 mg/kg)	
	Mct6$^{+/+}$	**Mct6$^{-/-}$**	**Mct6$^{+/+}$**	**Mct6$^{-/-}$**
CL[1] (mL/min/kg)	6.35	6.84	6.19	6.48
$A_{e,24\text{-}hr}$ (µg)	37.0 (22.8)	22.3 (3.87)	20.9 (2.82)	24.6 (2.62)
f_e	0.101 (0.019)	0.107 (0.007)	0.248 (0.139)	0.145 (0.021)
CL_R (mL/min/kg)	0.640 (0.122)	0.730 (0.048)	1.53 (0.857)	0.940 (0.138)
CL_{NR} (mL/min/kg)	5.71	6.11	4.66	5.54

Table 3: Summary of clearance parameters in Mct6$^{+/+}$ and Mct6$^{-/-}$ mice following 10 mg/kg i.v. (IV) and 25 mg/kg p.o. (PO) dose administrations. Data are reported as mean values ± S.D. [1]CL for oral administration was calculated as: $\mathrm{CL} = \mathrm{F} \cdot \mathrm{D}/\mathrm{AUC}_{0-\infty}$.

DMD Fast Forward. Published on June 25, 2020 as DOI: 10.1124/dmd.120.000068
This article has not been copyedited and formatted. The final version may differ from this version.

Figures

Fig. 1.

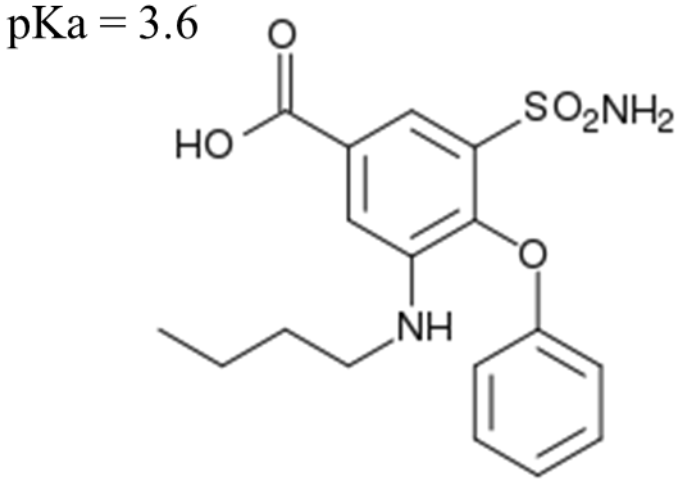

DMD Fast Forward. Published on June 25, 2020 as DOI: 10.1124/dmd.120.000068
This article has not been copyedited and formatted. The final version may differ from this version.

Fig. 2.

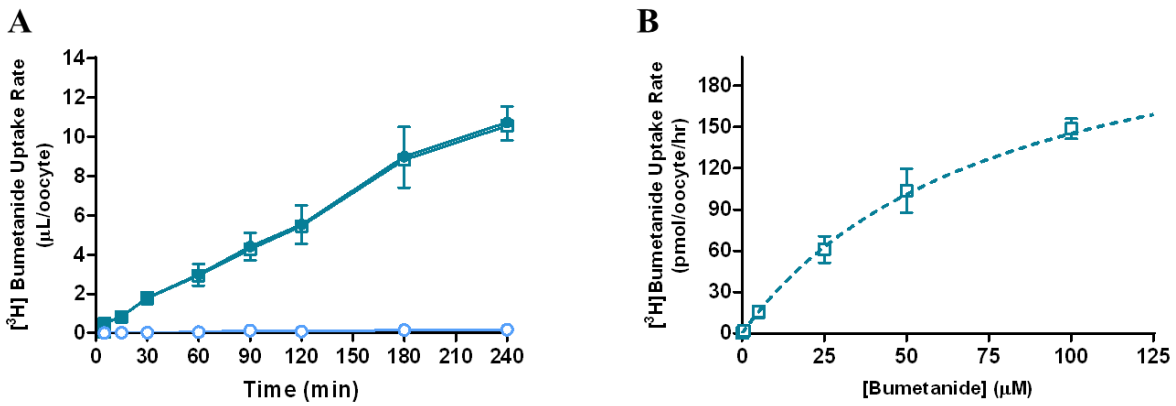

DMD Fast Forward. Published on June 25, 2020 as DOI: 10.1124/dmd.120.000068
This article has not been copyedited and formatted. The final version may differ from this version.

Fig. 3.

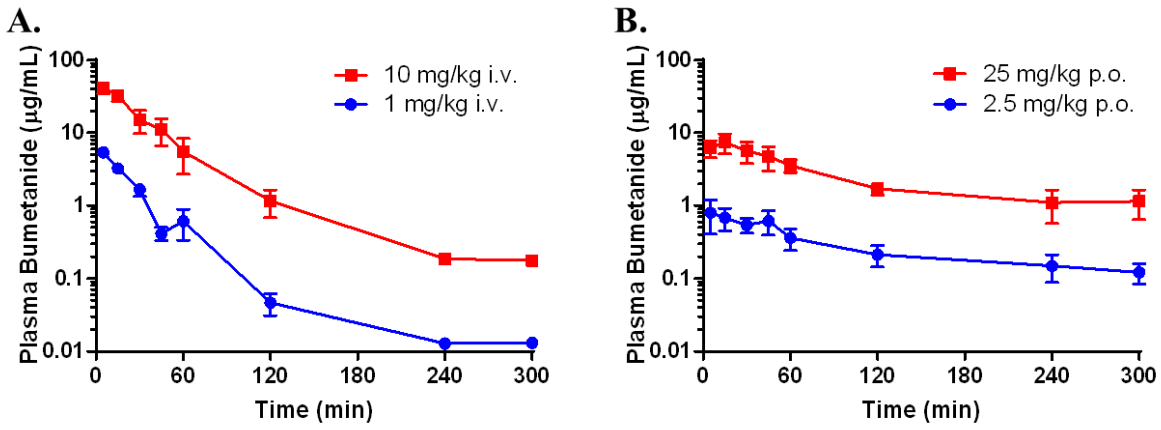

DMD Fast Forward. Published on June 25, 2020 as DOI: 10.1124/dmd.120.000068
This article has not been copyedited and formatted. The final version may differ from this version.

Fig. 4.

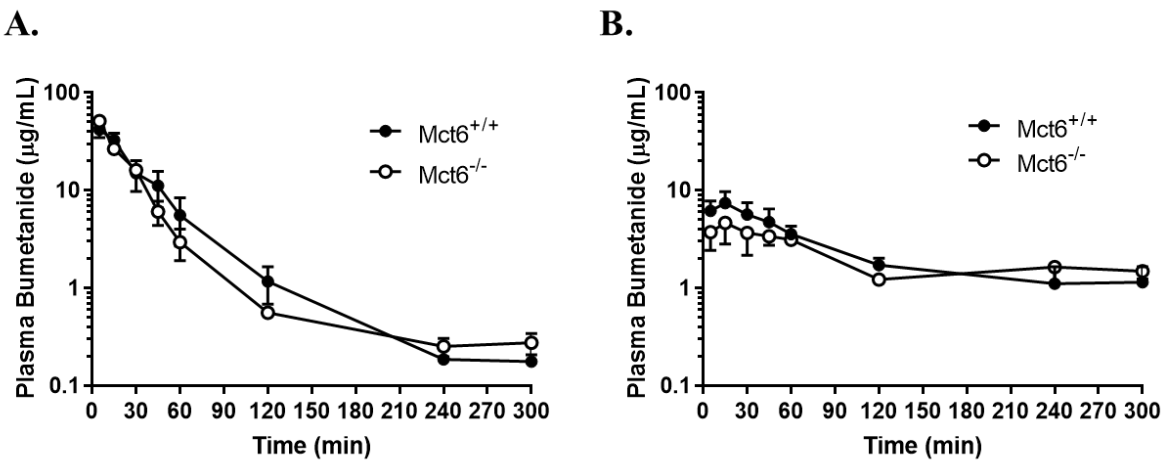

DMD Fast Forward. Published on June 25, 2020 as DOI: 10.1124/dmd.120.000068
This article has not been copyedited and formatted. The final version may differ from this version.

Fig. 5.

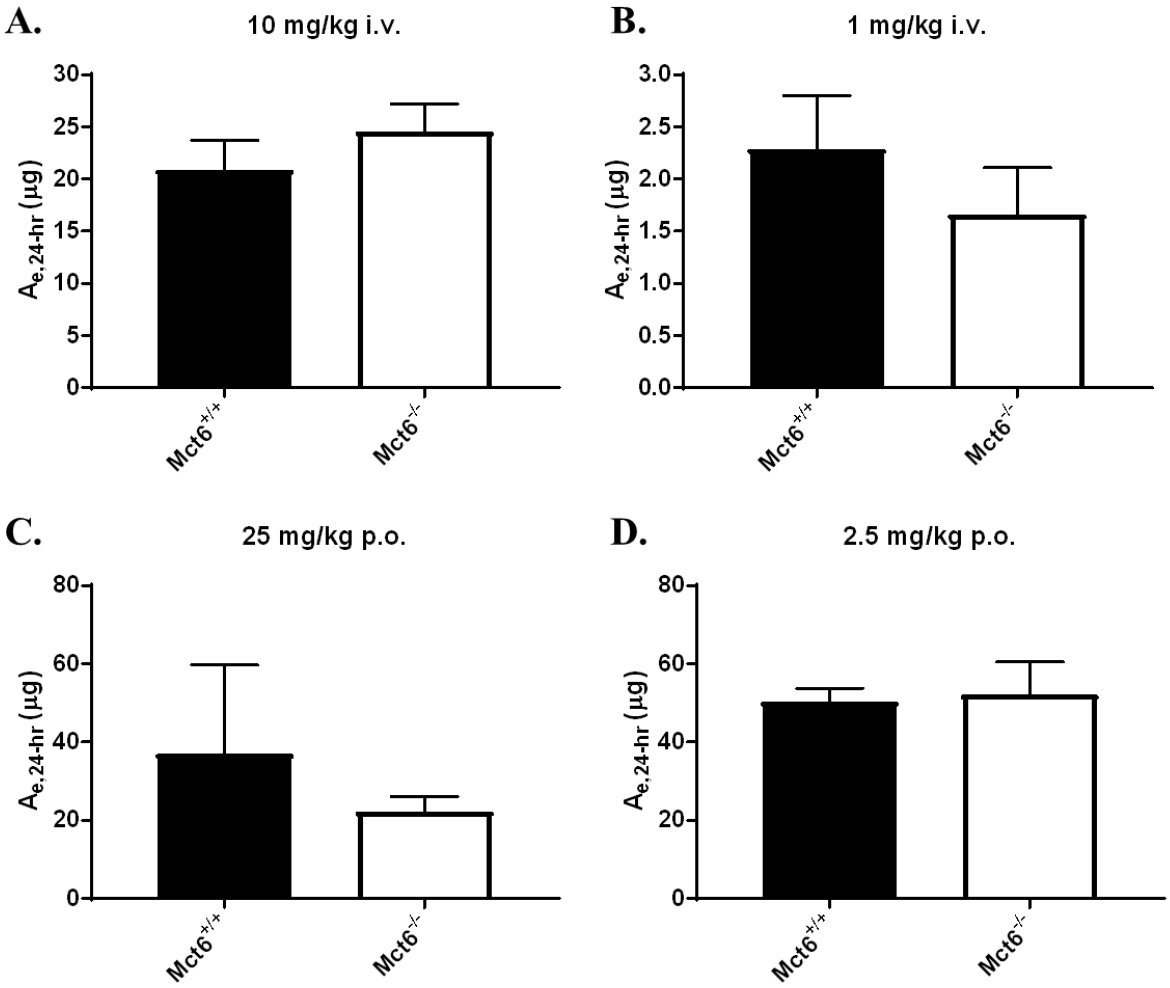

DMD Fast Forward. Published on June 25, 2020 as DOI: 10.1124/dmd.120.000068
This article has not been copyedited and formatted. The final version may differ from this version.

Fig. 6.

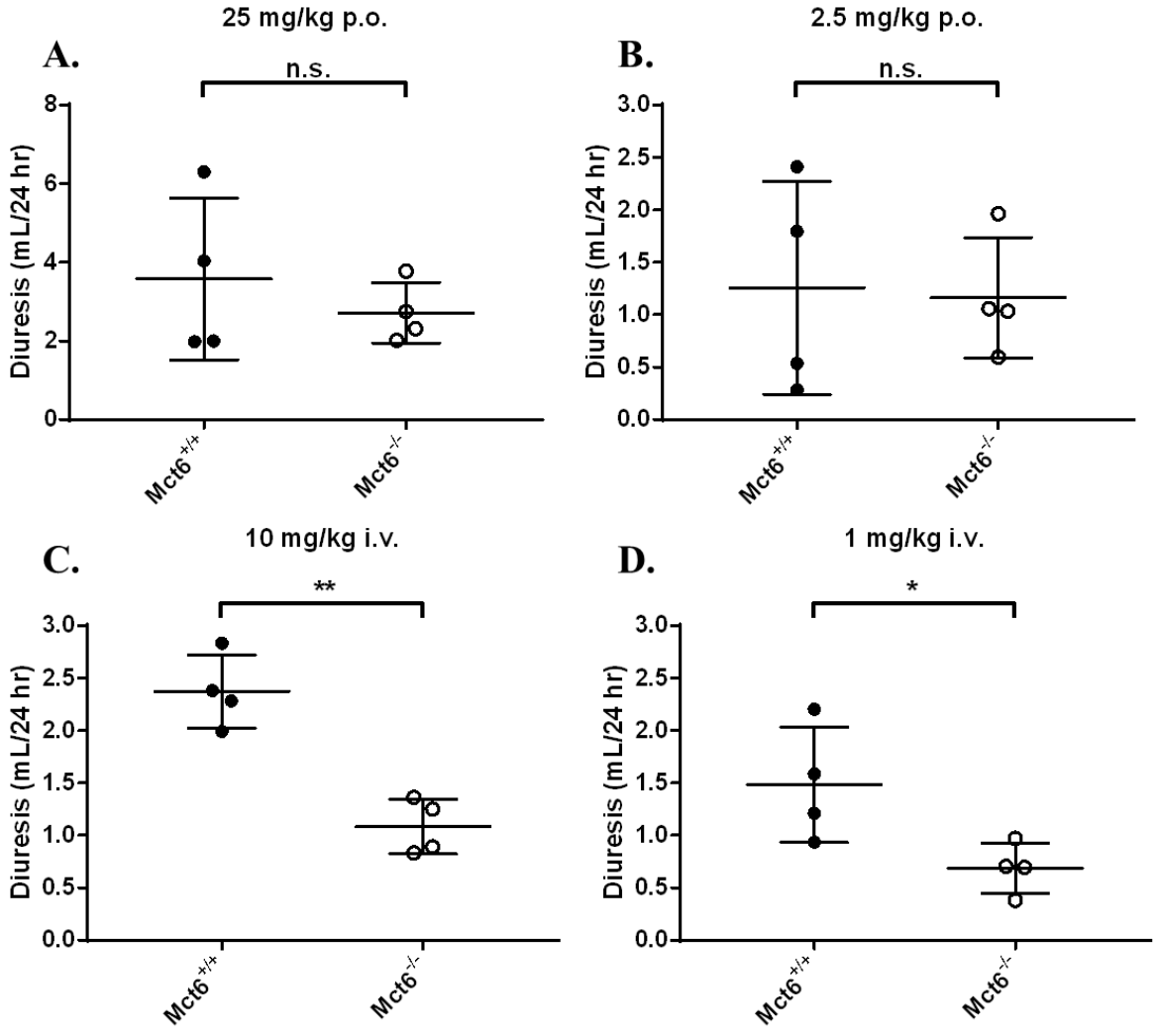

DMD Fast Forward. Published on June 25, 2020 as DOI: 10.1124/dmd.120.000068
This article has not been copyedited and formatted. The final version may differ from this version.

Fig. 7.